JOURNAL OF
Materials
CHEMISTRY

Pyrochlore–perovskite phase transformation in highly homogeneous (Pb,La)(Zr,Sn,Ti)O_3 powders

Joon-Hyung Lee*[a] **and Yet-Ming Chiang**[b]

[a]*Department of Inorganic Materials Engineering, Kyungpook National University, Taegu 702-701, Korea. E-mail: jhlee@icm.re.kr*
[b]*Department of Materials Science and Engineering, M.I.T., Cambridge, MA 02139, USA*

Received 28th June 1999, Accepted 8th October 1999

Control of undesirable pyrochlore is critical to the processing of lead perovskite dielectrics and ferroelectrics. In this work, a homogeneous and stoichiometric fine powder of the ferroelectric $Pb_{0.97}La_{0.02}(Zr_{0.64}Sn_{0.25}Ti_{0.11})O_3$ (PLZST) has been prepared by a hydroxide coprecipitation and freeze-drying method. Through systematic variation of processing temperature and time, we have characterized the pyrochlore-to-perovskite crystallization process of the powder. Studies of the crystallization behavior of the precursor as a function of temperature by X-ray powder diffraction and transmission electron microscopy showed that the pyrochlore phase forms from an amorphous precursor, initially at low temperatures around 500–550 °C. Further heat treatment to 750 °C resulted in development of the perovskite phase with no significant pyrochlore crystallite growth. At intermediate temperatures the precursor yielded a fine mixture of pyrochlore and perovskite phases. When the pyrochlore phase was heat-treated in air a slight weight increase was observed in the temperature range of 300–700 °C, which is attributed to oxygen absorption. The weight increase was not observed upon firing in argon atmosphere; instead, a weight loss occurred near 700 °C, which was identified as being mostly due to CO_2 gas evolution. This implies that the pyrochlore phase is crystallographically and thermodynamically metastable. An apparent activation energy of 53.9 kcal mol^{-1} was estimated for the pyrochlore–perovskite phase transformation.

Introduction

Pb(Zr,Ti,Sn)O_3 ceramics and their modifications have been studied for potential actuator applications using the antiferroelectric–ferroelectric phase transformation.[1–4] The electromechanical properties are directly related to the crystal chemistry, homogeneity and microstructure of these materials.[5,6] Generally, these ceramics have been prepared by the solid-state reaction of the constituent metal oxides and carbonates. Such reactions often lead to compositional and structural inhomogeneities in the final products.[7,8]

In Pb-based complex perovskites, PbO evaporates easily at high temperatures and forms undesirable phases.[9,10] The coexistence of an undesirable phase such as cubic pyrochlore, even in small amounts, deteriorates the ferroelectric properties.[11] Much effort has therefore been expended to eliminate the cubic pyrochlore phase. Usually 5–15 mol% of excess PbO are added to compensate PbO loss during heating,[12,13] and the columbite route which alters the reaction sequence and leads to almost pyrochlore free material is often employed.[14]

Recently, owing to increasing interest in ferroelectric films, the development of metastable pyrochlore and oxygen-deficient pyrochlore phases $A_2B_2O_7$ or $A_2B_2O_{7-\delta}$ at lower processing temperatures in Pb-containing thin films made by various methods has been reported.[15–17] According to some studies, the loss of PbO is the most important factor because local nonstoichiometry on the PbO-deficient side may promote pyrochlore formation.[18] To compensate for PbO loss, it has become common practice to use precursors with some excess PbO or, in the case of sputtering, to use targets containing up to 30% excess Pb (or PbO).[19] Other studies have shown the pyrochlore to be richer in Zr and more deficient in Pb than the perovskite phase.[20] The stronger tendency of Zr-containing compositions to form and retain the fluorite phase has been reported in the literature,[21] and is attributed to the tendency of Zr^{4+} to be coordinated by more than 6 oxygens, as is possible in the defect-fluorite structure. The oxygen partial pressure dependence of the pyrochlore–perovskite phase transformation has also been reported.[22–24] However, the mechanism of the phase transformation is still unclear as most of these studies have been reported in thin film processes.

In this study, ultra-fine stoichiometric and homogeneous ferroelectric PLZST powders were prepared by a coprecipitation and freeze-drying method. Powders prepared by solution precursor routes can be more homogeneous and reactive than those prepared by conventional solid-state reactions since the mixing of the reagents occurs on a finer scale.[25] Also, the lower processing temperatures that are usually possible minimize the loss of PbO by evaporation. The pyrochlore phase development during heating and the pyrochlore–perovskite phase transformation were analyzed using DTA-TG, ICP, mass spectrometry, XRD, TEM, and HRTEM.

Experimental

$Pb(NO_3)_2$ (99.9%), $La(NO_3)_3{\cdot}6H_2O$ (99.99%), $ZrOCl_2{\cdot}8H_2O$ (99.9%), $SnCl_4$ (99.99%) and $TiCl_4$ (99.999%) were used as starting chemicals. To prepare the Ti and Sn source solutions, $TiCl_4$ and $SnCl_4$ were dissolved in 30% aqueous H_2O_2 in a glove box to prevent the hydrolytic precipitation of each hydroxide, and the solutions were diluted to form a 0.1 mol dm^{-3} aqueous solution. $Pb(NO_3)_2$, $La(NO_3)_3{\cdot}6H_2O$ and $ZrOCl_2{\cdot}8H_2O$ were dissolved in distilled water individually and diluted to a concentration of 0.1 mol dm^{-3}. The mixed solution, corresponding to the composition $Pb_{0.97}La_{0.02}(Zr_{0.64}Sn_{0.25}Ti_{0.11})O_3$, was kept below pH 1 to avoid precipitation. Since PLZST ceramics are of interest for actuation based on the electric field-forced phase transformation from the antiferroelectric tetragonal (A_T) to the ferroelectric rhombohedral (F_R) phase,[26] a composition $Pb_{0.97}La_{0.02}(Zr_{0.64}Sn_{0.25}Ti_{0.11})O_3$ on the phase boundary between A_T and F_R phase was selected (Fig. 1). The

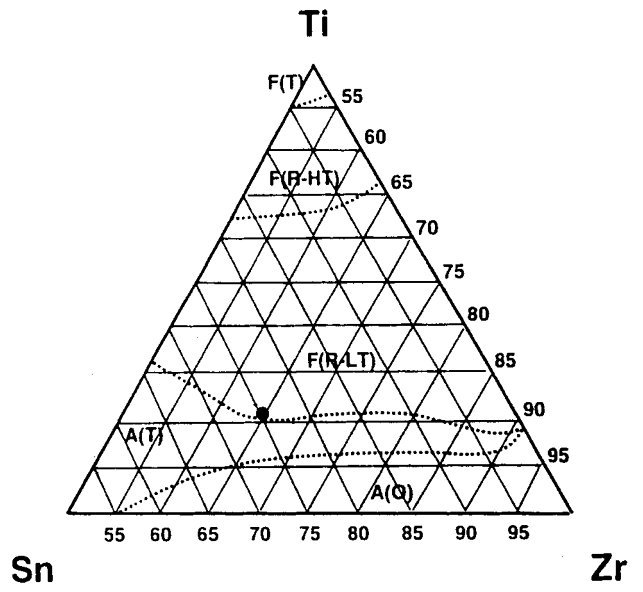

Fig. 1 Ternary phase diagram for the system $Pb_{0.97}La_{0.02}$(Zr, Sn, Ti)O_3 at 25 °C.[26]

PLZST solution was added dropwise to a continuously stirred bath of aqueous ammonia whose pH was adjusted to 9.

To compare the solubility behavior of individual metal hydroxides and to estimate the optimum coprecipitation conditions, the solubility diagrams for individual hydroxides are superimposed in Fig. 2.[27] In the pH range 5–6, Zr^{4+} and TiO^{2+} ions can be precipitated as hydroxides, but Pb^{2+} ions will remain dissolved as soluble species such as $Pb_6(OH)_8{}^{4+}$, or will be precipitated as chlorides in chloride media. In the basic pH domain of pH 10–11, Pb and Ti hydroxides can be precipitated, while $Zr(OH)_4$(s) will dissolve owing to the formation of soluble $Zr(OH)_5{}^-$ species. At pH 9 the Pb and Zr hydroxides can precipitate simultaneously along with the Ti hydroxide even though there are slight solubility differences between the hydroxides. Consequently, disregarding the formation of Pb chlorides or Pb carbonates, the optimum pH for the formation of a pure PLZST hydroxide precursor can be predicted, from the solubility diagrams, to be 9. Since the concentration of the corresponding metal solution was *ca.* 0.1 mol dm^{-3}, it was expected that >99% of metal hydroxide will precipitate at pH 9. During the coprecipitation, the pH of the bath was maintained at 9 by adding aqueous ammonia as necessary and the bath temperature was maintained at 60 °C in order to dissolve any Pb and Sn chlorides formed during the mixing process.

After the precipitation, the bath was cooled to room temperature and held for 1 hour for equilibration. Then the precipitate was separated by decantation of the supernatant liquid, and washed several times with a distilled water–NH_3 (aq) solution adjusted to pH 9, to remove residual Cl^- and $NO_3{}^-$ ions. The precipitate was sprayed into liquid nitrogen and freeze-dried in order to maintain chemical homogeneity and prevent powder agglomeration. The precipitate was then calcined at various temperatures for 1 hour. ICP analysis was used for elemental analysis of the calcined powders and also for determining the residual metal ion concentration in the decanted solution after precipitation. Powder X-ray diffraction with nickel-filtered Cu-Kα radiation (Rigaku RTP 500 RC) was used for phase identification. For lattice parameter measurement, a silicon standard powder (SRM 640B, NIST, USA) was added to the calcined powder. X-Ray diffractometry was performed with a step size of 0.002° and a counting time per step of 1 s. High temperature X-ray diffractometry (Rigaku RU 200) was used for kinetic analysis of the pyrochlore–perovskite phase transformation, scanning the main peaks of 222 and 012 for the pyrochlore and perovskite phases respectively. DTA–TG (Seiko, SSC/5200), mass spectrometry (Finnigan MAT 271), TEM (JEOL, JEM200CX) and HRTEM (ISI, EM002B) were also used for the characterization of powders.

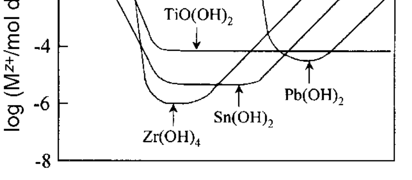

Fig. 2 Solubility diagram for the metal (Pb, Zr, Sn, Ti)–OH$^-$ system.[27]

Results and discussion

Fig. 3 shows the DTA–TG–DTG curves for the freeze-dried precipitates. The initial weight loss in the temperature range of 25–150 °C is attributed to the loss of surface-absorbed water, and is accompanied by a weak endothermic DTA peak. The marked weight loss at 200–430 °C in the DTA and TG traces is due to the decomposition of hydroxy groups and the appearance of endothermic peaks at 450 °C indicates the decomposition of $M(NO_3)_2$ into oxides as reported previously.[28] Therefore, complete decomposition was observed by around 450 °C.

ICP analysis was carried out for the powder calcined at 550 °C for 1 h and the results are shown in Table 1. The final composition was shifted a little into the F_R phase field.

Fig. 4 shows a series of X-ray diffraction patterns of the precipitate calcined at increasing temperatures for a fixed calcining time of 1 h. After the removal of hydroxy groups, solid-state mixing is believed to proceed. In the case of the sample calcined at 550 °C for 1 h, step scanning with a step size of 0.002° and a counting time per step of 1 s were used to obtain higher resolution X-ray diffraction patterns, and a magnified view of the diffraction peaks is shown. Broad peaks at positions corresponding to the pyrochlore phase and small superlattice peaks near $2\theta \approx 37°$ and 44° were observed. The powder at this stage consists of ultrafine particles of the pyrochlore phase ($A_2B_2O_{7-\delta}$). The particle size, calculated from X-ray peak broadening using the Scherrer equation,[29] was ≈6 nm. Because of peak broadening and the high background due to the ultrafine particle size, the superlattice reflections from the pyrochlore phase are barely detectable. At this stage of calcination, there exists a disordered fluorite solid solution. With increasing firing temperature, the perovskite PLZST

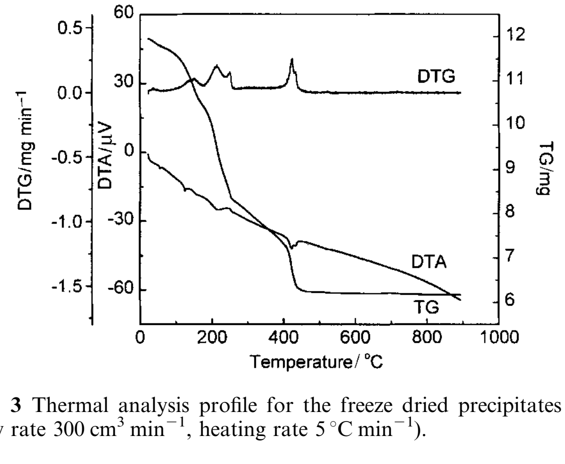

Fig. 3 Thermal analysis profile for the freeze dried precipitates (air flow rate 300 cm^3 min^{-1}, heating rate 5 °C min^{-1}).

Table 1 ICP chemical analysis of calcined powder

Element	Target composition (mol fraction)	Analyzed value (mol fraction)
Pb	0.970	0.983
La	0.020	0.006
Zr	0.640	0.631
Sn	0.250	0.251
Ti	0.110	0.128

phase begins to appear, and a single phase perovskite was obtained after firing at 750 °C for 1 h. At intermediate temperatures between 550 and 750 °C, the precursor yields a mixture of pyrochlore and perovskite phases.

The deconvoluted (202), (024) and (220) X-ray peaks corresponding to the rhombohedral phase are shown in Fig. 5. The calculated lattice parameters of the rhombohedral perovskite and cubic pyrochlore phases were $a_0 = 4.112$ Å, $\alpha = 89.838$, and $a_0 = 10.67$ Å, respectively.

Fig. 6 shows TEM micrographs illustrating the pyrochlore–perovskite phase development, from powders calcined at a) 450, b) 550 and c) 650 °C for 1 h. In Fig. 6a, the individual powder particles are about 8 nm in diameter and the selected area electron diffraction (SAED) pattern (Fig. 6a′) shows that it is a nearly amorphous phase. In Fig. 6b, the crystallite size is of the order of 5–8 nm, which matches well the calculated particle size from X-ray line broadening. The SAED of this powder (Fig. 6b′) shows several diffuse rings, from which the calculated *d*-spacings are close to those for the principal planes (*i.e.*, (222), (400), (440), and (622)) of a pyrochlore phase[30] with $c = 10.4$ Å. In the case of Fig. 6c, another new phase with crystallite size of the order of 50–200 nm was observed. This phase was identified by SAED to be the perovskite phase (Fig. 6c′).

HRTEM was used to investigate the nucleation process and morphological features of a sample calcined at 650 °C for 1 hour. Fine but agglomerated pyrochlore with an approximate crystallite size of 6 nm, and larger crystallites of the perovskite phase, are shown in Fig. 7. Both phases were well crystallized, and showed lattice fringe distances of 0.32 nm and 0.29 nm for the pyrochlore and perovskite phases, respectively. Compositional analysis of the pyrochlore and perovskite phases was conducted using energy dispersive X-ray spectroscopy (EDS) in the STEM. No differences were detected, however. For these chemically homogeneous powders prepared by the coprecipitation method, the compositions of the pyrochlore and perovskite phases appear to be identical except for the oxygen content, that is $A_2B_2O_6$ *vs.* $A_2B_2O_{7-\delta}$.

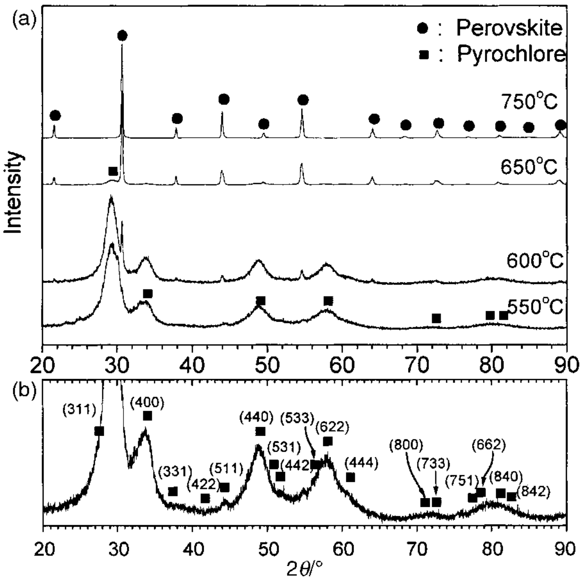

Fig. 4 (a) X-Ray diffraction patterns of the precipitates calcined at increasing temperatures for a fixed calcination time of 1 h, and (b) magnified view of the diffraction pattern of the sample calcined at 550 °C.

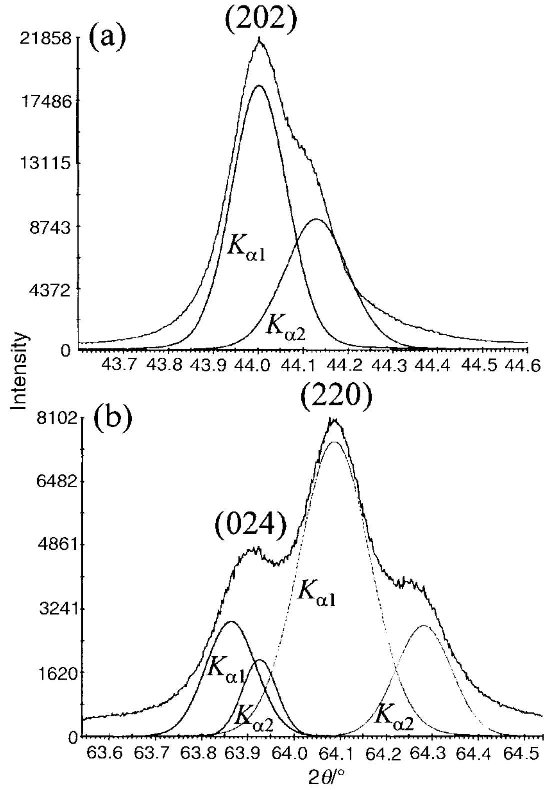

Fig. 5 Deconvoluted X-ray peaks of (a) (202) and (b) (024) and (220) corresponding to the rhombohedral crystal structure.

For a more detailed observation of thermogravimetric phenomena during heating, DTA–TG experiments were conducted in air and argon atmospheres for a pyrochlore

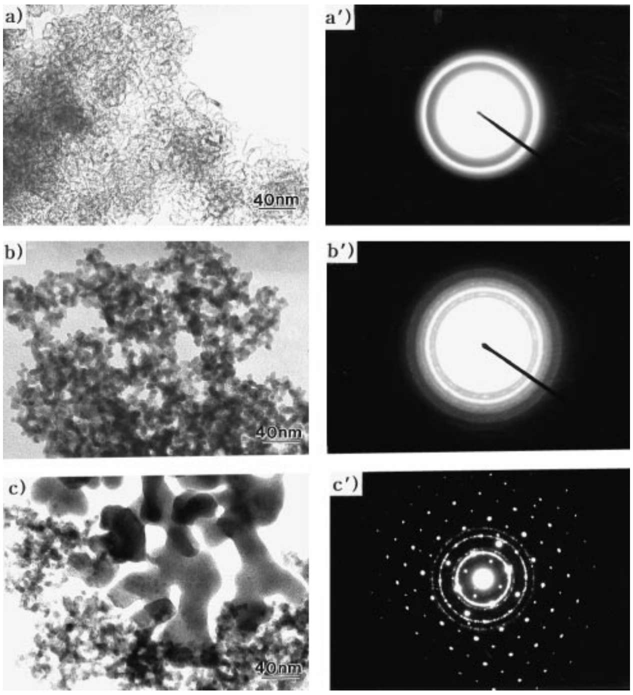

Fig. 6 TEM micrographs of pyrochlore–perovskite phase development of powders calcined at a) 450, b) 550 and c) 650 °C for 1 h, and the corresponding selected area electron diffraction (SAED) patterns (a′, b′, c′).

Fig. 7 HRTEM image of powder calcined at 650 °C for 1 h.

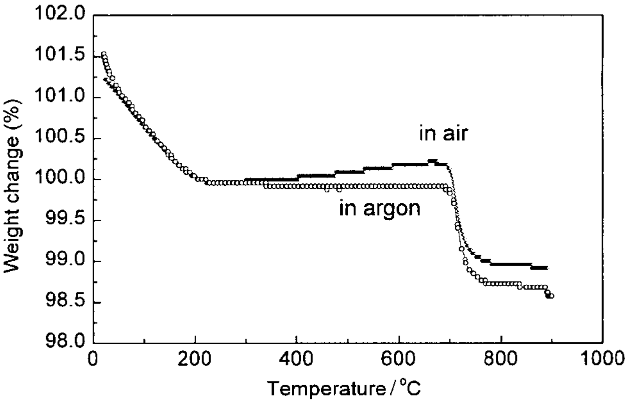

Fig. 8 TG analysis of pyrochlore phase powder in air and argon atmosphere (air and argon flow rates 300 cm^3 min^{-1}, heating ramp 5 °C min^{-1}).

phase powder obtained by calcining at 550 °C for 1 h (Fig. 8). The initial weight loss from room temperature to 200 °C is due to the evaporation of surface-absorbed water. Upon heating in air, an approximate 0.3% weight gain is observed between 200 and 680 °C and another weight loss of 1.3% is seen from 690 to 730 °C. In argon atmosphere, only the second weight loss, of 1.1% near 700 °C, appeared. A final slight weight loss above 830 °C for this sample may be due to the gradual evaporation of Pb.

Assuming that the pyrochlore PLZST phase has the ideal $A_2B_2O_7$ stoichiometry and transforms to the perovskite structure of stoichiometry $A_2B_2O_6$, a 2.27 wt% weight loss is expected from oxygen. The weight losses seen near 700 °C are considerably less than this value. This suggests that the pyrochlore phase crystallizing in the 200–550 °C range has an oxygen deficient stoichiometry $A_2B_2O_{7-\delta}$. For oxygen firing, the slight weight gain of 0.3% between 300 and 700 °C in Fig. 8 is attributed to some oxygen absorption, lowering δ. Furthermore, pyrolysis analysis using a gas mass spectrometer showed that the weight loss around 700 °C was caused by mostly CO_2 gas release. This indicates that the pyrochlore phase also contains residual carbon, further explaining why the weight loss during the pyrochlore to perovskite transformation is less than expected.

The pyrochlore–perovskite transformation requires heating to temperatures where long range diffusion becomes kinetically viable, reconstructing the cation as well as anion sublattices. During this process, excess oxygen and carbon are released and a corresponding weight loss is expected.

Previously reported results[22–24] on the effect of oxygen partial pressure on the perovskite phase formation, showing that calcining or annealing in oxygen atmosphere hinders the perovskite formation, can now be understood from the viewpoint of inhibition of oxygen release during the phase transformation.

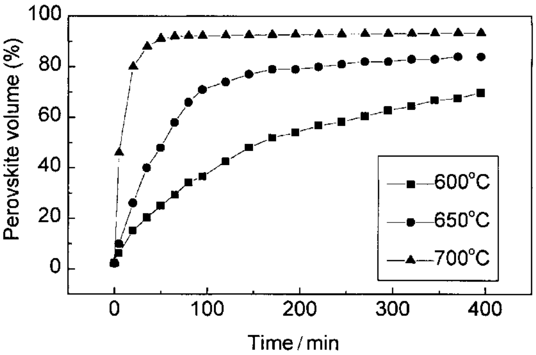

Fig. 9 Fractional perovskite PLZST as functions of time and temperature.

The kinetics for PLZST crystallization from the pyrochlore phase is shown for three different temperatures in Fig. 9. A Johnson–Mehl–Avrami analysis was performed on the kinetic data based on the following equation,[31,32]

$$\ln[-\ln(1-f)]=\ln(r)+m\ln(t) \qquad (1)$$

where f is the fraction crystallized isothermally at time t, r is the rate constant, which depends on the nucleation frequency and growth rate and is sensitive to temperature, and m is an exponent that is independent of temperature but sensitive to the reaction mechanism and the geometry of the particles. Hancock and Sharp[33] have shown that for reactions obeying a single theoretical rate expression, plots of $-\ln(\ln(1-f)$ against $\ln(t)$ over $f=0.15$–0.50 yield approximately straight lines with slopes m having values within certain ranges depending on the reaction mechanisms. When $m=0.54$–0.62, a diffusion controlled mechanism is indicated, while a zero-order, first-order, or phase-boundary controlled mechanism is indicated for $m=1.0$–1.24. A mechanism involving nucleation and growth control is indicated when $m=2.0$–3.0.

In Fig. 10, $-\ln(\ln(1-f))$ is plotted against $\ln(t)$ over a perovskite fraction $f=0.15$–0.50 from the data in Fig. 9. Linear regression yields an m value of 0.63–0.8, suggesting that the rate of reaction is diffusion-limited, in agreement with other literature on the bulk pyrochlore to perovskite phase transformation.[34]

An Arrhenius plot for the isothermal phase transformation from pyrochlore to perovskite is given in Fig. 11. The activation energy value obtained, 53.9 kcal mol^{-1}, which contains the activation energy for diffusion, is slightly lower than reported activation energies of 59–78 kcal mol^{-1} for pyrochlore–perovskite phase transformations in thin films.[16,35,36] These differences may be caused by the compositional differences between this and the thin film systems studied, and possibly also residual stresses in the case of thin films, which are absent in the present samples.[37]

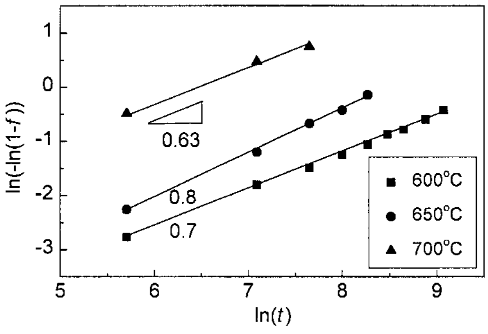

Fig. 10 Plot based on the Johnson–Mehl–Avrami analyses of the kinetic data from Fig. 9.

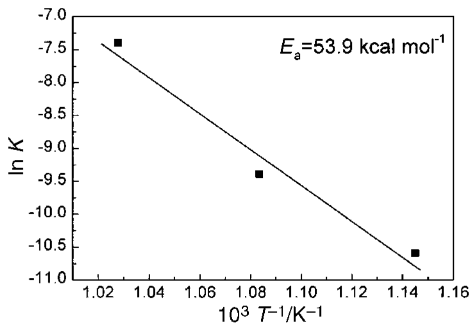

Fig. 11 Arrhenius plot for the isothermal phase transformation from pyrochlore to perovskite in PLZST. The activation energy is 53.9 kcal mol^{-1}.

Conclusions

Ultrafine PLZST powders were synthesized by a coprecipitation and freeze-drying method, and the crystallization behavior was characterized. The precursor is initially amorphous, and crystallizes to an oxygen-deficient pyrochlore phase of ≈6 nm crystallite size, containing residual carbon, over the temperature range 200–550 °C. Further heat treatment up to 750 °C resulted in a transformation to the perovskite phase with concurrent coarsening to a crystallite size of 50–200 nm. At intermediate temperatures the precursor yields a fine mixture of pyrochlore and perovskite phases. Detailed analysis of the pyrochlore phase using XRD, TG, mass spectrometry and HRTEM suggests that the pyrochlore phase is crystallographically and thermodynamically metastable. The perovskite powders prepared in this manner are much finer and more homogeneous than powders prepared by solid-state reaction. It was shown that the compositions of the pyrochlore and perovskite phases are identical except for the oxygen content. The activation energy for the pyrochlore to perovskite transformation is 53.9 kcal mol^{-1}, and Johnson–Mehl–Avrami analysis indicates that the process is diffusion-limited. It is suggested that this phase transformation scheme may be useful in preparing pyrochlore-free, homogeneous lead-based perovskite oxides.

Acknowledgements

This work was supported by ARO-MURI Contract No. DAAH04-95-1-0104, and used instrumentation supported by the MRSEC Program of the National Science Foundation under award number DMR 98-08941. This work was also supported by a post-doctoral fellowship from the Korea Science and Engineering Foundation (KOSEF).

References

1 W. Pan, Q. Zhang, A. Bhalla and L. E. Cross, *J. Am. Ceram. Soc.*, 1989, **72**, 571.
2 W. Y. Pan, C. Q. Dam, Q. M. Zhang and L. E. Cross, *J. Appl. Phys.*, 1989, **66**, 6014.
3 K. G. Brook, J. Chen, K. R. Udayakumar and L. E. Cross, *J. Appl. Phys.*, 1994, **75**, 1699.
4 K. Ghandi and N. W. Hagood, *Am. Inst. Aeronaut. Astronaut.*, 1994, **AIAA-94-1758-CP**, 221.
5 D. Viehland, D. Forst and J.-F. Li, *J. Appl. Phys.*, 1994, **75**, 4137.
6 G. Arlt, D. Hennings and G. de With, *J. Appl. Phys.*, 1985, **58**, 1619.
7 J. Thomson, Jr., *Am. Ceram. Soc. Bull.*, 1974, **53**, 421.
8 C. D. Chandler, C. Roger and M. J. Hampden-Smith, *Chem. Rev.*, 1993, **93**, 1205.
9 R. L. Holman and R. M. Fulrath, *J. Appl. Phys.*, 1973, **44**, 5227.
10 T. Tani and D. A. Payne, *J. Am. Ceram. Soc.*, 1994, **77**, 1242.
11 B. Tuttle, R. W. Schwartz, D. H. Doughty and I. A. Voigt, in *Ferroelectric Thin Films*, ed. E. R. Myers and A. I. Kingon, Materials Research Society, Pittsburgh, PA, 1990, p. 159.
12 B. A. Tuttle, J. A. Voigt, D. C. Goodnow, D. L. Lamppa, T. J. Headley, M. O. Eatough, G. Zeuder, R. D. Nasby and S. M. Rodgers, *J. Am. Ceram. Soc.*, 1993, **76**, 1537.
13 J. F. Chang and S. B. Desu, *J. Mater. Res.*, 1994, **9**, 955.
14 S. L. Swartz and T. R. Shrout, *Mater. Res. Bull.*, 1982, **17**, 1245.
15 S. A. Mansour, G. L. Liedl and R. W. Vest, *J. Am. Ceram. Soc.*, 1995, **78**, 1617.
16 C. K. Kwok and S. B. Desu, in *Ceramic Transactions Vol. 25: Ferroelectric Films*, ed. A. S. Bhalla and K.M. Nair, American Ceramic Society, Westerville, OH, 1992, p. 85.
17 C. H. Peng and S. B. Desu, *J. Am. Ceram. Soc.*, 1994, **77**, 1486.
18 M. Ishida, H. Matsunami and T. Tanaka, *J. Appl. Phys.*, 1997, **48**, 951.
19 K. Iijima, R. Takayama, Y. Tomita and I Ueda, *J. Appl. Phys.*, 1986, **60**, 2914.
20 A. H. Carim, B. A. Tuttle, D. H. Doughty and S. L. Martinez, *J. Am. Ceram. Soc.*, 1991, **74**, 1455.
21 A. Siefert, F. F. Lange and J. S. Speck, *J. Mater. Sci.*, 1995, **10**, 680.
22 L. A. Bursill and K. G. Brooks, *J. Appl. Phys.*, 1994, **75**, 4501.
23 G. R. Fox and S. B. Krupanidhi, *J. Mater. Res.*, 1994, **9**, 699.
24 K. G. Brooks, I. M. Reaney, R. Klissurska, Y. Huang, L. Bursill and N. Setter, *J. Mater. Res.*, 1994, **9**, 2540.
25 R. Roy, *Science*, 1987, **238**, 1664.
26 D. Berlincourt, *IEEE Trans. Sonics Ultrasonics*, 1966, **13**, 116.
27 C. F. Baes, Jr. and R. E. Mesmer, *The Hydrolysis of Cations*, John Wiley & Sons, New York, 1976.
28 K. L. Yadav and R. N. P. Choudhary, *J. Mater. Sci.*, 1993, **28**, 765.
29 B. D. Cullity, *Elements of X-ray Diffraction*, Addison-Wesley Publishing Co., Inc., Massachusetts, 1978, p. 102.
30 C. K. Kwok and S. B. Desu, *Appl. Phys. Lett.*, 1992, **60**, 1430.
31 M. Avrami, *J. Chem. Phys.*, 1939, **7**, 1103.
32 M. Avrami, *J. Chem. Phys.*, 1941, **9**, 177.
33 J. D. Hancock and J. H. Sharp, *J. Am. Ceram. Soc.*, 1972, **55**, 74.
34 H. M. Jang, S. R. Cho and K. M. Lee, *J. Am. Ceram. Soc.*, 1995, **78**, 297.
35 E. M. Griswold, L. Weaver, I. D. Calder and M. Sayer, *Mater. Res. Soc. Symp. Proc.*, 1995, **361**, 389.
36 Y. Yoshikawa and K. Tsuzuki, *J. Am. Ceram. Soc.*, 1990, **73**, 31.
37 S. Y. Chen, C. M. Wang and S. Y. Cheng, *J. Am. Ceram. Soc.*, 1991, **74**, 2506.

Paper 9/05142B